# Structure and enhanced antimicrobial activity of mechanically activated nano TiO$_2$

Vera P. Pavlović[a], Jelena D. Vujančević[b], Pavle Mašković[c], Jovana Ćirković[d], Jelena M. Papan[e], Darko Kosanović[b], Miroslav D. Dramićanin[e], Predrag B. Petrović[f], Branislav Vlahović[g,h], Vladimir B. Pavlović[b]*

[a]University of Belgrade, Faculty of Mechanical Engineering, Belgrade, Serbia

[b]Institute of Technical Sciences of SASA, Belgrade, Serbia

[c]University of Kragujevac, Faculty of Agronomy, Čačak, Serbia

[d]University of Belgrade, Institute for Multidisciplinary Research, Belgrade, Serbia

[e]University of Belgrade, Vinča Institute of Nuclear Sciences, Vinča, Belgrade, Serbia

[f]University of Kragujevac, Faculty of Technical Sciences Čačak, Čačak, Serbia

[g]North Carolina Central University, Durham, NC, USA

[h]NASA University Research Center for Aerospace Device Research and Education and NSF Center of Research Excellence in Science and Technology Computational Center for Fundamental and Applied Science and Education, Durham, NC, USA

* Corresponding author. *E-mail address*: vladimir.pavlovic@itn.sanu.ac.rs

## Abstract

Titanium dioxide is a photocatalyst, known not only for its ability to oxidise organic contaminants, but also for its antimicrobial properties. In this article, significant enhancement of the antimicrobial activity of TiO$_2$ (up to 32 times) was demonstrated after its activation by ball milling. The antimicrobial activity was analyzed for one fungal and 13 bacterial ATCC strains using the microdilution method and recording the minimum inhibitory concentration

(MIC) values. In order to further investigate the correlation between the mechanical activation of $TiO_2$ and its antimicrobial activity, the structure, morphology and phase composition of the material were studied by means of Electron Microscopy, X-ray diffraction and nitrogen adsorption-desorption measurements. UV-Vis diffuse reflectance spectra were recorded and the Kubelka-Munk function was applied to convert reflectance into the equivalent band gap energy ($E_g$) and, consequently, to investigate changes in the $E_g$ value. X-ray photoelectron spectroscopy was used to analyse the influence of mechanical activation on the Ti 2p and O 1s spectra. The presented results are expected to enable the development of more sustainable and effective advanced $TiO_2$-based materials with antimicrobial properties that could be used in numerous green technology applications.

**Keywords:** titanium dioxide, mechanical activation, structure, spectroscopy, antimicrobial activity

## 1. Introduction

The worldwide industrial production growth imposes high demands on the development of new economically sustainable and efficient solutions for increased environmental pollution. Among environmental hazards, microbial populations are an exceptional threat to humans, especially in crowded indoor environments. Moreover, the emergence of antibiotic-resistant bacteria increases the risk and requires the use of novel and more potent antibacterial agents. Nanomaterials with exclusive photocatalytic properties may ensure adequate sanitation of environmentally contaminated surfaces and spaces, since nanoparticles can be used as self-consistent antimicrobial agents, in an aqueous suspension, or as coating layers for a common material surface[1-3]. Silver, ZnO and CuO nanoparticles have an important effect against microbial growth, but their utilization is restricted since they may pose a hazard to other

2

organisms when they are released into the environment [4]. Reports on the application of $TiO_2$ as a photocatalyst in wastewater treatment, food industry, pharmacy, medicine, indoor environments and in development of new self-cleaning and antimicrobial materials, point out the advantages of utilization of this material due to its low cost and the fact that it does not pose a significant threat to the environment and human health[5-10]. Literature data indicate that $TiO_2$ is highly stable and that the oxidation of organic compounds involving this material is environmentally friendly, free from any secondary pollutants as final reaction products[11].

$TiO_2$ can occur in several crystal phases, but under the ambient conditions, three phases are common: thermodynamically stable rutile (tetragonal, $P4_2/mnm$), and two metastable phases — anatase (tetragonal, $I4_1/amd$) and brookite (orthorhombic, $Pbca$). According to the literature data, anatase shows better photocatalytic properties than rutile, although rutile has a narrower energy band gap[12-15, 4]. However, this mainly applies to cases where there are no noteworthy differences in other structural parameters, such as particle size, crystallographic orientation on the surface of the material, defect concentration, differences in surface amorphization, etc. Nevertheless, surface characteristics can play an important role in the adsorption of molecules and the charge transfer, as well as in the involvement of charge carriers in redox reactions on the surface of its particles, which also determines photocatalytic properties[15]. Crystal lattice defects, such as oxygen or titanium vacancies, affect the processes of trapping charge carriers, not only on their way to the surface, but also on the surface itself. Thus, the electrons photoexcitated from the valence to the conduction band can be trapped in the formation of $Ti^{3+}$ centers. If the holes photogenerated into the valence band reach the surface, they may be trapped by the $H_2O$ molecules at the surface, or by surface titanol groups, thereby producing surface adsorbed hydroxyl radicals. The electrons that reach the surface of the particles react with the electron acceptor species that are present on the particle surface, as well as with oxygen in the air. For example, electrons from the conducting zone

reduce oxygen by creating reactive superoxide ions ($O_2^{\bullet-}$), which jointly with other highly reactive oxygen species (ROS), such as hydroxyl radical ($^{\bullet}OH$), hydroperoxyl radical ($HO_2^{\bullet}$), hydrogen peroxide ($H_2O_2$) etc., act photocatalytically and antimicrobially[2, 4, 16, 17]. Some reports on photocatalytic activity indicate that the amorphous $TiO_2$ particles exhibit worse photocatalytic properties, due to a high number of defects inside the volume of the photocatalyst. The defects can act as sites for the recombination of photo-generated electron-hole pairs, preventing them from participating in catalytic redox reactions on the surface of the catalyst[18-20]. These results show that achieving a higher degree of crystallinity is essential in the synthesis. Nevertheless, other literature data indicate that the existence of an amorphous rutile layer on the surface of crystalline nanoparticles increases photocatalytic activity[14], due to a higher concentration of surface active sites. It is also reported that a mixture of different polymorphic $TiO_2$ phases can have a synergistic effect and can lead to improved photocatalytic activity[15]. However, some studies show that the best results in terms of the photocatalytic effect are achieved in the presence of anatase as the dominant phase and the presence of rutile up to about 30 %[21, 22], while others suggest that the prevalence of rutile and a low presence of anatase can result in a stronger photocatalytic activity and a stronger antimicrobial effect[23]. Very few authors emphasize the importance of brookite[24].

The aforementioned literature data refer partly to $TiO_2$ thin films[4, 15, 23, 24] and partly to $TiO_2$ nanoparticles[1, 2, 12-14, 16, 21, 22]. As far as the latter are concerned, it may be observed that nanoparticles have mostly been obtained via hydrolysis and hydrothermal reactions, as well as by the solvothermal method, a modified sol-gel method and aerosol flame synthesis. This usually involves expensive precursors, careful atmosphere control, the limitation to cation solutions with similar solubility products, etc. Therefore, the use of other, simpler methods, such as mechanical activation, can be of interest for producing nanocrystalline powders, including $TiO_2$. Mechanical activation is an effective inexpensive method for obtaining

highly dispersed powders with a modified structure, morphology and surface activity[25]. This also includes a possible transfer between different polymorph modifications of the starting powder, induced both by mechanical stress and the local increase of heat during mechanical activation. Bearing in mind the previous review of the important, though insufficiently clarified role of different $TiO_2$ crystal modifications in determining the photocatalytic and antimicrobial activity of $TiO_2$, mechanical activation may appear as a powerful method not only for obtaining $TiO_2$ nanoparticles, but also for tailoring their photocatalytic and antimicrobial properties. The literature data regarding the correlation between the antimicrobial activity of $TiO_2$ and the structure modifications induced by mechanical activation of the material are scarce. Therefore, in this article, the influence of the mechanical activation of $TiO_2$ powder on structural changes and the resulting antimicrobial properties is analyzed.

## 2. Experimental Procedure

Commercially available powder of titanium (IV) oxide (99.5 % purity, Sigma-Aldrich) was mechanically activated in a planetary ball-mill (Fritsch Pulverisette 5) for 10, 30 and 60 minutes, at 300 rpm, in a $ZrO_2$ jar (500 cm$^3$) with $ZrO_2$ balls of 10 mm in diameter. The powder-to-ball ratio was 1:40. After performing mechanical activation, the powders were dispersed in distilled water, ultra-sonicated for 10 minutes and dried at 100 °C for 24 hours. The samples were denoted as $TiO_2$-0 (non-activated), $TiO_2$-10, $TiO_2$-30 and $TiO_2$-60 (activated for: 10, 30 and 60 minutes, respectively).

The morphology and microstructure changes resulting from the mechanical activation were recorded by a Scanning Electron Microscope (SEM, JOEL JSM-6390 LV) and a Transmission Electron Microscope (TEM, JEM-1400).

The characterizations of the phase composition and the crystal structure of the $TiO_2$ powders were monitored using X-ray diffraction (XRD), with a step of 0.01° and an acquisition rate of 1°/min, using a Rigaku SmartLab diffractometer with $CuK_\alpha$ radiation. The International Centre for Diffraction Data (ICDD) database was used for the detection of crystal phases. The nitrogen adsorption-desorption isotherms were determined using a Micromeritics ASAP 2020 instrument. The samples were degassed at 150 °C for 10 hours under reduced pressure. The specific surface area of the samples was calculated according to the Brunauer-Emmett-Teller (BET) method from the linear part of the nitrogen adsorption isotherms. The total pore volume was taken at $p/p_0 = 0.998$, where p and $p_0$ represented the equilibrium and saturation pressures of nitrogen at the adsorption temperature. The mesopore volume was calculated according to the Barrett-Joyner-Halenda (BJH) method, from the desorption branch of the isotherm. The volume of micropores was calculated from alpha-S plot.

The XPS measurements were conducted on a Kratos Axis Ultra XPS system with Monochromated Al $K_\alpha$ X-Rays (1486.6 eV). All survey scans were collected with the pass energy of 160 eV, while all region scans were done with the pass energy of 20 eV. The C 1s peak at 284.5 eV was used for the calibration of the spectra. Component fitting was performed with a Shirley background.

The UV-Vis diffuse reflectance spectra (DRS) were recorded using a Shimadzu UV-2600 spectrophotometer, in the interval of 300–750 nm. The reflectance spectra were measured relative to $BaSO_4$ as a reference sample.

Minimum inhibitory concentrations (MIC) of the extract and cirsimarin against one fungal and 13 bacterial ATCC strains were determined using the microdilution method in 96 multi-well microtiter plates[26]. All tests were performed in the Muller–Hinton broth (MHB) with the exception of yeast, in which case the Sabouraud dextrose broth was used. A volume of 100 μL stock solutions of cirsimarin (in 10 % DMSO, 2 mg/mL) was pipetted into the first row of

the plate. Fifty microliters of Mueller–Hinton or Sabouraud dextrose broth (supplemented with Tween 80 at the final concentration of 0.5% (v/v) for the analysis of oil) were added to the other wells. A volume of 50 µL from the first test wells was pipetted into the second well of each microtiter line, and then 50 µL of the scalar dilution was transferred from the second to the twelfth well. Ten µL of the resazurin indicator solution (prepared by dissolving a 270-mg tablet in 40 mL of sterile distilled water) and 30 µL of the nutrient broth were added to each well. Finally, 10 µL of the bacterial suspension ($10^6$ CFU/mL) and the yeast spore suspension ($3 \times 10^4$ CFU/mL) were added to each well. The growth conditions and the sterility of the medium were checked, for each strain. The standard antibiotic amracin was used to control the sensitivity of the tested bacteria, while Nystatin was applied as a control against the tested yeast. Plates were first wrapped loosely with cling film to ensure that bacteria did not become dehydrated and then prepared in triplicate. After that, they were placed in an incubator at 37 °C for 24 hours for the bacteria and at 28 °C for 48 hours for the yeast. Any change of color, from purple to pink, or colorless, was recorded as positive. The lowest concentration at which color change occurred was taken as the MIC value. The average of three values was calculated and the obtained value was taken as the MIC for the tested compounds and standard drug. Since the beginning of mixing, throughout the incubation period, the system was illuminated using a UVA lamp (Super ultra violet fluorescent lantern UVPUVL4F) with $\lambda = 368$ nm, from the distance of 30 cm.

## 3. Results and discussion

### 3.1. XRD analysis

Changes in the crystal structure of the $TiO_2$ powder induced by mechanical activation were identified using XRD measurements and they are shown in Figure 1. All diffraction lines

typical of the anatase crystal modification are present in the analyzed range of the XRD diffractogram of the non-activated powder. A small amount of rutile is also detected. Figure 1 shows that even the short activation for 10 minutes results in a significant change in the diffraction pattern. The intensity of all anatase reflections rapidly decreases and some of them disappear. The intensity of the peak dominantly originating from the strongest anatase line (101) becomes comparable with the intensity of the strongest rutile line (110). All rutile lines generally increase, and the rutile line (211) appears to be dominant at the position where the clearly exposed anatase (105) and (211) lines were previously detected. Very weak hints of other rutile lines also occur in $TiO_2$-10. A wide and weak peak at the position ~ 31.3° corresponds to one of the two strongest lines of the brookite crystal modification. Since the brookite phase, which is orthorhombic, is metastable at ambient pressure and can be obtained in the polymorphic transformation of anatase at elevated pressures, it can be concluded that increased stress values and defect concentration during mechanical activation contributed to the reduced value of the minimum critical pressure required for the transition from anatase to brookite[27].

During the activation for 30 min the weight fraction of anatase further decreases and the strongest line of rutile (110) begins to dominate the entire diffraction pattern (Figure 1). However, the intensity of rutile lines in $TiO_2$-30 is very similar to the intensity of the corresponding lines in the diffraction spectrum of the sample $TiO_2$-10. Namely, since decreased mean crystallite sizes and increased microstrains caused by mechanical activation generally lead to a decreased intensity of the diffraction lines and to the their widening, a larger amount of the rutile fraction in the powder is not accompanied with the appearance of more intense and sharper lines of rutile. For the same reason, no rise in the intensity of brookite lines has been noticed. Among the anatase diffraction lines, only the strongest one is observed, with the possible contribution of two brookite lines at that position.

The diffraction analysis of $TiO_2$ powder obtained after the activation for 60 min indicates that the rutile phase is the dominant in the mixture of three phases, while the amount of anatase is almost negligible. It can be concluded that some amount of brookite is transferred to rutile when the activation time is longer than 10–30 minutes. The observed brookite-to-rutile transformation is in accordance with the results published by Begin-Colin et al. and Penn and Banfierld[28, 29]. In fact, this is in line with the assumption that the general direction of mechanically induced polymorphic transformation of titanium dioxide can largely be described as the transitions "anatase $\rightarrow$ brookite $\rightarrow$ rutile". The Rietveld refinement method was applied to the diffraction patterns of all samples. The weight percentages of $TiO_2$ phases and their structure parameters are presented in Table 1.

### 3.2. Microstructure analyses

In order to determine the influence of the employed mechanical activation on the morphology and size of powder particles, SEM and TEM analyses were conducted. It can be observed (Figure 2) that non-agglomerated particles in the non-activated powder predominantly have a spherical shape. They form agglomerates with the size distribution in the 100– 900 nm range, where the highest probability of occurrence is noticed for the agglomerates with the diameter in the range 300 nm < d < 500 nm (Fig. S1). Due to mechanical activation, the size of agglomerates and non-agglomerated particles has changed. Short activation (10 minutes) has strongly reduced the proportion of agglomerates with a diameter above 200 nm, leading to the highest occurrence probability for the agglomerates with the diameter between 150 nm and 200 nm. On the other hand, the activation that lasted for 30 minutes or longer has led to noticeable secondary agglomeration, thereby increasing the mean diameter of agglomerates up to 240–260 nm (Fig. S1). Namely, the secondary agglomeration of milled particles occurs

as a pronounced effect due to a higher surface activity of particles, leading to the renewed presence of larger agglomerates.

The size of non-agglomerated particles, obtained using TEM measurements, decreases not only for short activation time, but also for prolonged activation (Fig. S2 and Table 2). The presented results obtained by using electron microscopy are in accordance with the measurements of the specific surface area, pore volume and pore diameter of the samples (Table 3). It can be seen that mechanical activation leads to the increase in the specific surface area ($S_{BET}$) of the powder, compared to the $TiO_2$-0 sample. The occurrence of secondary agglomeration, due to an increase in the particle surface energy during comminution of the initial powder particles, causes the slight reduction of $S_{BET}$ value for the prolonged activation, with respect to the value for the $TiO_2$-10 sample. Furthermore, the applied mechanical activation decreases the total pore volume and the mesopore volume, as well as the mean pore diameter.


### 3.3. Optical properties

The optical properties of all $TiO_2$ samples were investigated using a UV-Vis diffuse reflectance spectroscopy (Fig. S3). The Kubelka-Munk function was applied to convert reflectance into the equivalent band gap energy. Figure 3 shows the plot of $[F(R)h\nu]^{1/2}$ vs. $h\nu$, where linear segments are extended to intersect with abscissa, in order to determine the influence of mechanical activation on band gap energies ($E_g$). The determined $E_g$ values indicate that the energy of band gap decreases for 0.08 eV after 10 minutes of activation, while further activation leads to a very slight decrease (0.01 eV) in $E_g$. The observed $E_g$ shift can be attributed to the resulting impact of various structure alterations: a higher weight percentage of rutile, the reduction in the size of non-agglomerated particles, and a higher amount of surface defects (such as oxygen vacancies or $Ti^{3+}$ centers) created during

mechanical activation. It should be noticed that the diminishing of non-agglomerated particles may even result in the opposite change in the band gap value, if the mean particle size drops below a critically low value[30]. The $E_g$ values obtained for prolonged mechanical activation can be explained in this context.

**3.4. XPS analysis**

XPS measurements were performed to study the surface state changes induced by mechanical activation, primarily concerning the chemical state of titanium and the changes in oxygen composition. The regular splitting of the Ti 2p region[31] into two main peaks, Ti $2p_{3/2}$ at ~ 458.8 eV and Ti $2p_{1/2}$ at ~ 464.5 eV, is observed in the high-resolution XPS spectrum of the non-activated powder (Figure 4a). The positions of both Ti 2p peaks, as well as their symmetric form, indicate the domination of the $Ti^{4+}$ state in the sample[32, 33]. A slight decrease in the binding energy of these peaks is noticed for the activated powders. According to the literature data[33, 34], this decrease can be attributed to the weak partial conversion of $Ti^{4+}$ to $Ti^{3+}$, associated with the increased presence of other point defects, such as oxygen vacancies. The latter assumption is in accordance with the observed shift in the $E_g$ value (Figure 3), since the oxygen vacancy states between the valence and conduction bands can cause a shift in UV-Vis spectra towards the visible spectra. The shoulder at 462.45 eV in the $TiO_2$-10 may also be considered as an additional evidence for the assumed $Ti^{3+}$ presence[35, 36], but there are no clearly noticeable $Ti^{3+}$ peaks within the Ti $2p_{3/2}$ region of BE. It is noteworthy that the asymmetry of the Ti $2p_{3/2}$ peak is clearly pronounced for the sample activated for 30 minutes (Figure 4a). Since the XPS peak of Ti 2p in the ideal stoichiometric $TiO_2$ is generally not a broad peak and has no shoulder[37], this asymmetry may indicate the occurrence of nonstoichiometry introduced by the mechanical activation. On the other hand, the presence of three different $TiO_2$ modifications can also influence the shape and the position of Ti 2p

spectra in the activated $TiO_2$ samples. From this point of view, the decrease in the BE value of the Ti $2p_{3/2}$ peak with the mechanical activation can be interpreted as a result of the polymorph phase transition from anatase to rutile during activation[38].

The O 1s spectra of all samples are shown in Figure 4b. In the non-activated $TiO_2$ (almost pure anatase) and in the samples with the longest activation time (the highest percentage of rutile, with a negligible share of anatase), the O 1s spectrum fits well with two components. The component with a lower binding energy corresponds to oxygen in the O—Ti bonds (lattice oxygen), while the other can be attributed to the active surface oxygen species (hydroxyl-like groups, chemisorbed oxygen, adsorbed molecular water, or oxygen species with carbon related to the air contaminants) ($O_{ads}$ in Figure 4b)[30, 39]. For the O 1s spectra of the samples $TiO_2$-10 and $TiO_2$-30, where the presence of brookite as an additional (intermediate) phase is prominent, the best fit is achieved using three or four components in the deconvolution. Actually, instead of one component originating from the surface oxygen species, two or three final components of this type appear in the spectra. This is primarily caused by the fact that activation leads to decreased particle sizes and increased defect concentration and surface activity. Namely, the amount of adsorbed oxygen and water, and consequently the concentration of superoxide ions and hydroxyl radicals, may increase due to mechanical activation and the consequent intensification of surface activity. This is most probably the case with the $TiO_2$-10 sample, where secondary agglomeration is not pronounced. Since the agglomeration process becomes prominent in the samples activated for a longer time, it causes deterioration in the particle surface activity and changes the previous trend in developing the O 1s effect. The decreased area of the lattice oxygen O 1s peak ($O_{latt}$), relative to the total area of O 1s, may also indicate the formation of some oxygen vacancies in the lattice, which is usually related to the occurrence of $Ti^{3+}$ [40].

### 3.5. Antimicrobial analysis

Figure 5 shows the results of the analysis of the antimicrobial activity of the non-activated and mechanically activated $TiO_2$. Investigations were performed on one fungal and 13 bacterial ATCC strains, where the bacterial strains included both Gram negative and Gram positive bacteria (Figure 5). The results obtained using the microdilution method reveal a significant change in the inhibitory activity to tested microorganisms, that is a remarkable drop in the MIC values, when the mechanically activated $TiO_2$ was used. For some of the tested cultures of microorganisms MIC values dropped from 625 µg/mL to 78.12, 39.10, or even to 19.53 µg/mL (Figure 5a). Thus, a significantly higher antimicrobial activity, up to 32 times, was reached. Even in the two types of bacteria where the weakest antimicrobial effect was achieved the MIC was reduced to 1/8 of its original value (Figure 5c).

According to the experimental data, it can be concluded that the test materials based on the activated $TiO_2$ have shown a high antimicrobial activity towards tested bacteria in a pH neutral environment. Therefore, it can be assumed that the contact between the $TiO_2$ particles and bacteria leads to the damage of the cell wall and the cell membrane. The degradation of the cell membrane and the loss of its permeability are the main reasons for the destruction of bacteria[10]. By connecting to ribosomes (30S and 50S ribosomal subunits) $TiO_2$ particles may inhibit the translation of genetic information and the synthesis of proteins, subsequently leading to the destruction of bacteria (bacteriostatic and bactericide effect). $TiO_2$ particles may also bond with the A subunit of DNA gyrase, thereby blocking the effect of this enzyme which is essential for the DNA replication. This causes a direct damage of the DNA molecule of bacteria. The effect is bactericide. The antifungal action of the activated $TiO_2$ particles is explained by the fact that particles bond with the ergosterol molecules in the fungal membrane and cause the formation of cavities, which leads to an increased permeability of

the membrane, destroying the membrane integrity and causing its odour (fungistatic and fungicide effect).

As far as the change of the MIC values versus the time of mechanical activation of $TiO_2$ (Figure 5) is concerned, it can be seen that a sharp increase in antimicrobial activity, shown as the steepest reduction in the MIC values, was detected for the $TiO_2$-10 sample. Having in mind that the SEM, TEM and XRD results indicate that even the activation time of 10 minutes results in a significant decrease in the mean particle and crystallite size and that the XRD results reveal a transition of anatase into the rutile phase via brookite, a remarkable improvement in the antimicrobial effect of the $TiO_2$-10 relative to the $TiO_2$-0 sample can be associated primarily: a) with the synergistic photocatalytic and antimicrobial effect of various polymorphic modifications and b) with the reduction of the mean particle size and an increased active particles surface. The last conclusion is in accordance with the obtained increase in the specific surface area. As already mentioned, the XPS results do not indicate the essential formation of $Ti^{3+}$ centers within the crystal lattice. Consequently, there is no noteworthy trapping of electrons that would further affect the photocatalytic and antimicrobial activity. On the other hand, a significant increase in the surface area of the part of the O1s peak assigned to active surface oxygen species may be observed (Figure 4b), which is directly related to better antimicrobial properties, compared to the non-activated sample.

The influence of all these effects is also present in $TiO_2$-30, although with a smaller area of the total $O_{ads}$1s effect in the XPS spectrum, due to the pronounced secondary agglomeration of the powder particles. Further reduction in the size of crystallites and non-agglomerated particles takes place (Tables 1 and 2). It should be mentioned that the partial amorphization of the particle surface area can also be assumed, since it commonly occurs during the milling process[41]. This might contribute to the observed enhanced antimicrobial activity in 13 out of

the 14 studied microbial cultures. Figure 4 suggests that the XPS phenomena related to the generation of surface $^\bullet OH$ and $HO_2^\bullet$ radicals are especially pronounced in the samples $TiO_2$-10 and $TiO_2$-30. Taking into consideration that hydroxyl radicals usually cause oxidation of phospholipids within the membrane of microbial cells when the cells adhere to the surface of the $TiO_2$ catalyst, inducing thereby the loss of membrane integrity[11], it is expected that the samples $TiO_2$-10 and $TiO_2$-30 may show a major increase in the antimicrobial activity. It has also been reported that $^\bullet OH$ radicals not only act on $TiO_2$ surface, but also diffuse over short distances through the surrounding solution, consequently degrading organic compounds that are not in direct contact with the photocatalyst[1]. However, as far as the dependence of the MIC on the activation time (Figure 5) is concerned, it may be observed that the antimicrobial activity change rate is slightly lower (ie the degree of change in antimicrobial activity is lower) when activation time increases from 10 to 30 minutes than when it increases from 0 to 10 minutes. These results are in accordance with the confirmed dependence of the band gap energy value on the time of the mechanical activation of $TiO_2$.

An enhanced antimicrobial activity with the further prolongation of mechanical activation up to 60 minutes is observed in 7 out of the 14 cultures of microorganisms, but the degree of the increase of antimicrobial activity is less pronounced than in the samples activated for a shorter time. This is caused by the more intensive secondary agglomeration in the powder activated for the longest time, and by the fact that the synergistic effect of the joint photocatalytic and antimicrobial activities of various polymorphic modifications is not prominent, since the weight share of brookite has declined considerably and the percentage of the remaining anatase is almost negligible.


**4. Conclusions**

15

This paper shows that even a short mechanical activation can remarkably enhance the antimicrobial activity of $TiO_2$, due to the impact on the structure, morphology and phase composition of the starting material. XRD measurements revealed that mechanical activation led to the phase transformation from anatase to rutile, via brookite, with the reduction of the mean crystallite size and increased microstrain. It was concluded that the weight percentages of the anatase and rutile phases were approximately equal in the sample activated for 10 minutes, resulting in a synergistic effect in terms of the photocatalytic and antimicrobial activity.

Microstructure analyses confirmed the breaking of initial agglomerates, the decreased mean diameter of non-agglomerated particles and the significantly higher value of the specific surface area due to short mechanical activation, which additionally increased photocatalytic activity. The energy of band gap decreased for 0.08 eV. The shift observed for the activated $TiO_2$ samples, compared to pristine $TiO_2$, was attributed to the joint impact of various structure alterations: the higher weight percentage of rutile, the reduced size of non-agglomerated particles, the higher specific surface area of the powder and a higher amount of surface defects created during mechanical activation. XPS investigations revealed an important change in the high-resolution spectra of $TiO_2$ activated for 10 minutes. This primarily refers to the peaks obtained by fitting the O 1s spectra, assigned to an active surface oxygen species, including surface oxygen of the adsorbed oxygen species, weakly bonded oxygen and hydroxyl-like groups. The XPS phenomena related to generating the $^{\bullet}OH$ and $HO_2^{\bullet}$ radicals were especially pronounced. Less distinct changes were observed for the samples subjected to the longer activation, due to secondary agglomeration and the related modifications in surface activity, causing the change from a steep to a slight decline of the MIC value. Generally, the results obtained using the microdilution method showed that a remarkably enhanced antimicrobial activity was achieved for all examined cultures of

microorganisms (one fungal and 13 bacterial ATCC strains) due to the mechanical activation of $TiO_2$. Namely, for some of the tested cultures of microorganisms the minimum inhibitory concentration (MIC) values dropped from 625 μg/mL to 78.125, 39.1, or even to 19.53 μg/mL, when the $TiO_2$ sample with the longest activation time was used. Thus, significantly higher antimicrobial activity, up to 32 times, was reached. Even in the two types of bacteria where the weakest antimicrobial effect was achieved, the MIC value was reduced to 1/8 of its original value. The obtained results enable the further development of coatings, films and nanocomposites based on mechanically activated nano $TiO_2$, which could be used for the antimicrobial protection of various types of solid surfaces.

**References**

1. De Falco G, Porta A, Petrone AM, et al. Antimicrobial Activity of Flame-Synthesized Nano-$TiO_2$ Coatings. Environ. Sci. Nano. 2017;4:1095-1107.

2. Hirakawa K, Mori M, Yoshida M, Oikawa S, Kawanishi S. Photo-irradiated titanium dioxide catalyzes site specific DNA damage via generation ofhidrogen peroxide. Free. Radic. Res. 2004;38:439-447.

3. Ditta IB, Stelle A, Liptrot C, et al. Photocatalytic antimicrobial activity of thin surface films of $TiO_2$, CuO and $TiO_2$/CuO dual layers on *Escherichia coli* and bacteriophage T4. Appl. Microb. Cell Physiol. 2008;79:127-133.

4. Joost U, Juganson K, Visnapuu M, et al. Photocatalytic antibacterial activity of nano-TiO$_2$ (anatase)-based thin films: effects on Escherichia coli cells and fatty acids. J. Photochem. Photobiol. B, Biol. 2015;142:178−185.

5. Banerjee S, Dionysiou D, Pillai SC. Self-cleaning applications of TiO$_2$ by photo-induced hydrophilicity and photocatalysis. Appl. Catal. B. 2015;176;396–428.

6. Carp O, Huisman CL, Reller A. Photoinduced reactivity of titanium dioxide. Prog. Solid State Chem. 2004;32;33-177.

7. Weir A, Westerhoff P, Fabricius L, Hristovski K, Von Goetz N. Titanium dioxide nanoparticles in food and personal care products. Environ. Sci. Technol. 2012;46(4):2242-50.

8. Zhao J, Yang X. Photocatalytic oxidation for indoor air purification: a literature review. Build. Environ. 2003;38;645-654.

9. Chong MN, Jin B, Chow CWK, Saint C. Recent developments in photocatalytic water treatment technology: A review. Water Res. 2010;44:2997-3027.

10. Lan Y, Lu Y, Ren Z. Mini review on photocatalysis of titanium dioxide nanoparticles and their solar applications. Nano Energy. 2013;2;1031–1045.

11. Markov SL, Vidaković AM. Testing Methods for Antimicrobial Activity of TiO$_2$ Photocatalyst. APTEFF. 2014;45:141-151.

12. Kang M, Lee SY, Chung CH, et al. Characterization of a TiO$_2$ photocatalyst synthesized by the solvothermal method and its catalytic performance for CHCl$_3$ decomposition. J. Photochem. Photobiol. A, Chem. 2001;144:185–191.

13. Su C, Hong B-Y, Tseng C-M. Sol–gel preparation and photocatalysis of titanium dioxide. Catal. Today. 2004;96:119–126.

14. Krivec M, Segundo RA, Faria JL, Silva AMT, Dražić G. Low-temperature synthesis and characterization of rutile nanoparticles with amorphous surface layer for photocatalytic degradation of caffeine. Appl. Catal. B. 2013;140–141:9–15.

15. Luttrell T, Halpegamage S, Tao J, Kramer A, Sutter E, Batzill M. Why is anatase a better photocatalyst than rutile? - Model studies on epitaxial $TiO_2$ films. Sci. Rep. 2014;4:4043-1-7.

16. Sun DS, Kau JH, Huang HH, Tseng YH, Wu WS, Chang HH. Antibacterial Properties of Visible-Light-Responsive Carbon-Containing Titanium Dioxide Photocatalytic Nanoparticles against Anthrax. Nanomaterials. 2016; 6:237- 1-12.

17. Li Z, Cong S, Xu Y. Brookite vs Anatase $TiO_2$ in the Photocatalytic Activity for Organic Degradation in Water. ACS Catal. 2014;4:3273−3280.

18. Ohtani B, Ogawa Y, Nishimoto S. Photocatalytic Activity of Amorphous-Anatase Mixture of Titanium (IV) Oxide Particles Suspended in Aqueous Solutions. J. Phys. Chem. B. 1997; 101:3746-3752.

19. Nosaka Y, Nosaka A. Introduction to Photocatalysis - From Basic Science to Applications. Cambridge, UK: The Royal Society of Chemistry; 2016.

20. Zhang J, Cong Y, Anpo M. Chemical Methods for the Preparation of Multifunctional Photocatalysts. In: Anpo M, Kamat PV, eds. Environmental Benign Photocatalysts: Applications of Titanium Oxide-based Materials, New York: Springer Science & Business Media, 2010: 7-34.

21. Bakardijeva S, Šubrt J, Štengl V, Dianez MJ, Sayagues MJ. Photoactivity of anatase–rutile $TiO_2$ nanocrystalline mixtures obtained by heat treatment of homogeneously precipitated anatase, Appl. Catal. B. 2005;58:193–202.

22. Bacsa RR, Kiwi J. Effect of rutile phase on the photocatalytic properties of nanocrystalline titania during the degradation of p-coumaric acid. Appl. Catal. B. 1998;16:19-29.

23. Vymětalová V, Jelínek M, Písařík P, Mikšovský J, Remsa J, Řasová V. Antibacterial Activity Of Titanium Dioxide and Ag-Incorporated DLC Thin Films, Lékař a technika. 2016;3:65–68.

24. Addamo M, Bellardita M, Di Paola A, Palmisano L. Preparation and photoactivity of nanostructured anatase, rutile and brookite $TiO_2$ thin films. Chem. Commun. 2006;47:4943–4945.

25. Pavlović VP, Popović D, Krstić J, Dojčilović J, Babić B, Pavlović VB. Influence of Mechanical Activation on the Structure of Ultrafine $BaTiO_3$ powders. J. Alloys Compd. 2009;486:633-639.

26. Sarker SD, Nahar L, Kumarasamy Y. Microtitre plate based antibacterial assay incorporating resazurin as indicator of cell growth, and its application in the in vitro antibacterial screening of phytochemicals. Methods. 2007;42:321-324.

27. Rezaee M, Khoie SMM, Liu KH. The role of brookite in mechanical activation of anatase-to-rutile transformation of nanocrystalline $TiO_2$: An XRD and Raman spectroscopy investigation. Cryst. Eng. Comm. 2001;13:5055-5061.

28. Bégin-Colin S, Girot T, Le Caër G, Mocellin A. Kinetics and Mechanisms of Phase Transformations Induced by Ball-Milling in Anatase $TiO_2$. J. Solid State Chem. 2000;149:41–48.

29. Penn RL, Banfield JF. Formation of rutile nuclei at anatase 112 twin interfaces and the phase transformation mechanism in nanocrystalline titania. Am. Mineral. 1999;84:871–876.

30. Lin H, Huang CP, Li W, et al. Size dependency of nanocrystalline $TiO_2$ on its optical property and photocatalytic reactivity exemplified by 2-chlorophenol. Appl. Catal. B. 2006;68:1–11

31. Sanjines R, Tang H, Berger H, Gozzo F, Margaritondo G, Levy F. Electronic structure of anatase $TiO_2$ oxide. J. Appl. Phys. 1994;75:2945–2951.

32. Liu B, Wen QHL, Zhao X. The effect of sputtering power on the structure and photocatalytic activity of $TiO_2$ films prepared by magnetron sputtering. Thin Solid Films. 2009;517:6569–6575.

33. Byrne C, Fagan R, Hinder S, McCormack DE, Pillai SC. New Approach of Modifying the Anatase to Rutile Transition Temperature in $TiO_2$ Photocatalysts. RSC Adv. 2016;6:95232-95238.

34. Georgios P, Wolfgang SM. X-Ray Photoelectron Spectroscopy of Anatase-$TiO_2$ Coated Carbon Nanotubes. Solid State Phenom. 2010;162:163-177.

35. Luciu I, Bartali R, Laidani N. Influence of hydrogen addition to an Ar plasma on the structural properties of $TiO_{2-x}$ thin films deposited by RF Sputtering. J. Phys. D: Appl. Phys. 2012;45.345302-345-1-9.

36. Fu Y, Du H, Zhang S, Huang W. XPS characterization of surface and interfacial structure of sputtered TiNi films on Si substrate. Mater. Sci. Eng., A. 2005,403:25–31.

37. Xiong LB, Li JL, Yang B, Yu Y. $Ti^{3+}$ in the Surface of Titanium Dioxide: Generation, Properties and Photocatalytic Application. J. Nanomater. 2012;2012:831524-1-13.

38. Scanlon DO, Dunnill CW, Buckeridge J, et al. Band alignment of rutile and anatase $TiO_2$. Nature Mater. 2013;12:798–801.

39. Jensen H, Solovyev A, Lie Z, Søgaard EG. XPS and FTIR investigation of the surface properties of different prepared titania nano-powders. Appl. Surf. Sci. 2005;246:239-249.

40. Bharti B, Kumar S, Lee HN, Kumar R. Formation of oxygen vacancies and Ti$^{3+}$ state in TiO$_2$ thin film and enhanced optical properties by air plasma treatment. Sci. Rep. 2016;6:32355-1-12.

41. Lee GJ, Park EK, Yang SA, Park JJ, Bu SD, Lee MK. Rapid and direct synthesis of complex perovskite oxides through a highly energetic planetary milling. Sci. Rep. 2017; 7:46241.

**Figure captions**

Figure 1. XRD patterns of non-activated and mechanically activated TiO$_2$ (A – anatase, R – rutile, B – brookite)

Figure 2. SEM micrographs of TiO$_2$-0 (a), TiO$_2$-10 (b), TiO$_2$-30 (c) and TiO$_2$-60 (d)

Figure 3. Tauc plot of the transformed Kubelka-Munk function versus photon energy, for non-activated and mechanically activated TiO$_2$

Figure 4. a) Ti 2p and b) O 1s high resolution XPS spectra of non-activated and mechanically activated TiO$_2$. Mark $\Delta$ stands for BE(2p$_{1/2}$)-BE(2p$_{3/2}$), while marks O$_{latt}$, O$_{ads}$ and O$_{tot}$ refer to the lattice oxygen, surface oxygen species and total oxygen in the material, respectively

Figure 5. The influence of the mechanical activation of TiO$_2$ on the MIC values of the extract and cirsimarin against the tested microorganisms

**List of Tables:**

Table 1. Weight percentage, crystal structure parameters, mean crystallite size and microstrain values of different phases in non-activated and mechanically activated $TiO_2$, obtained using the Rietveld refinement method

| Sample | Phases | wt (%) | Unit cell parameters (Å) | | | Unit cell volume ($Å^3$) | Mean crystallite size (nm) | Microstrain (%) |
|---|---|---|---|---|---|---|---|---|
| | | | a | b | c | | | |
| | anatase | 91.2 | 3.782 | 3.782 | 9.506 | 135.969 | 27.35 | 0.16 |
| $TiO_2$-0 | rutile | 8.8 | 4.593 | 4.593 | 2.957 | 62.325 | 18.00 | 0.25 |
| | orthorhombic | - | - | - | - | - | - | - |
| | anatase | 26 | 3.787 | 3.787 | 9.516 | 136.472 | 15.00 | 0.60 |
| $TiO_2$-10 | rutile | 25 | 4.598 | 4.598 | 2.959 | 54.862 | 10.67 | 0.29 |
| | orthorhombic | 49 | 4.525 | 5.500 | 4.940 | 122.944 | 2.17 | 1.66 |
| | anatase | 8 | 3.789 | 3.789 | 9.536 | 136.904 | 12.30 | 0.64 |
| $TiO_2$-30 | rutile | 46 | 4.601 | 4.601 | 2.958 | 62.618 | 8.90 | 0.14 |
| | orthorhombic | 46 | 4.561 | 5.534 | 4.966 | 125.344 | 2.40 | 1.45 |
| | anatase | 5 | 4.138 | 4.138 | 8.730 | 149.484 | 2.15 | 1.91 |
| $TiO_2$-60 | rutile | 62 | 4.597 | 4.597 | 2.957 | 62.488 | 6.72 | 0.44 |
| | orthorhombic | 33 | 4.502 | 5.588 | 5.008 | 125.987 | 1.59 | 2.30 |

Table 2. The influence of the mechanical activation on the diameter of agglomerates and non-agglomerated particles

| Activation time (min) | SEM results | | TEM results | |
|---|---|---|---|---|
| | Mean diameter of agglomerates (nm) | Median diameter of agglomerates (nm) | Mean diameter of non-agglomerated particles (nm) | Median diameter of non-agglomerated particles (nm) |
| 0 | 422 | 397 | 45 | 44 |
| 10 | 174 | 159 | 26 | 25 |
| 30 | 240 | 208 | 17 | 17 |
| 60 | 256 | 210 | 13 | 13 |

Table 3. The influence of the mechanical activation on the structural parameters obtained from the nitrogen adsorption-desorption isotherms: the specific surface area ($S_{BET}$), the total pore volume ($V_{tot}$), the mesopore and micropore volume ($V_{meso}$ and $V_{micro}$), the mean pore diameter ($D_{mean}$) and the pore diameter where the maximum of the derivative cumulative volume curve is reached ($D_{max}$)

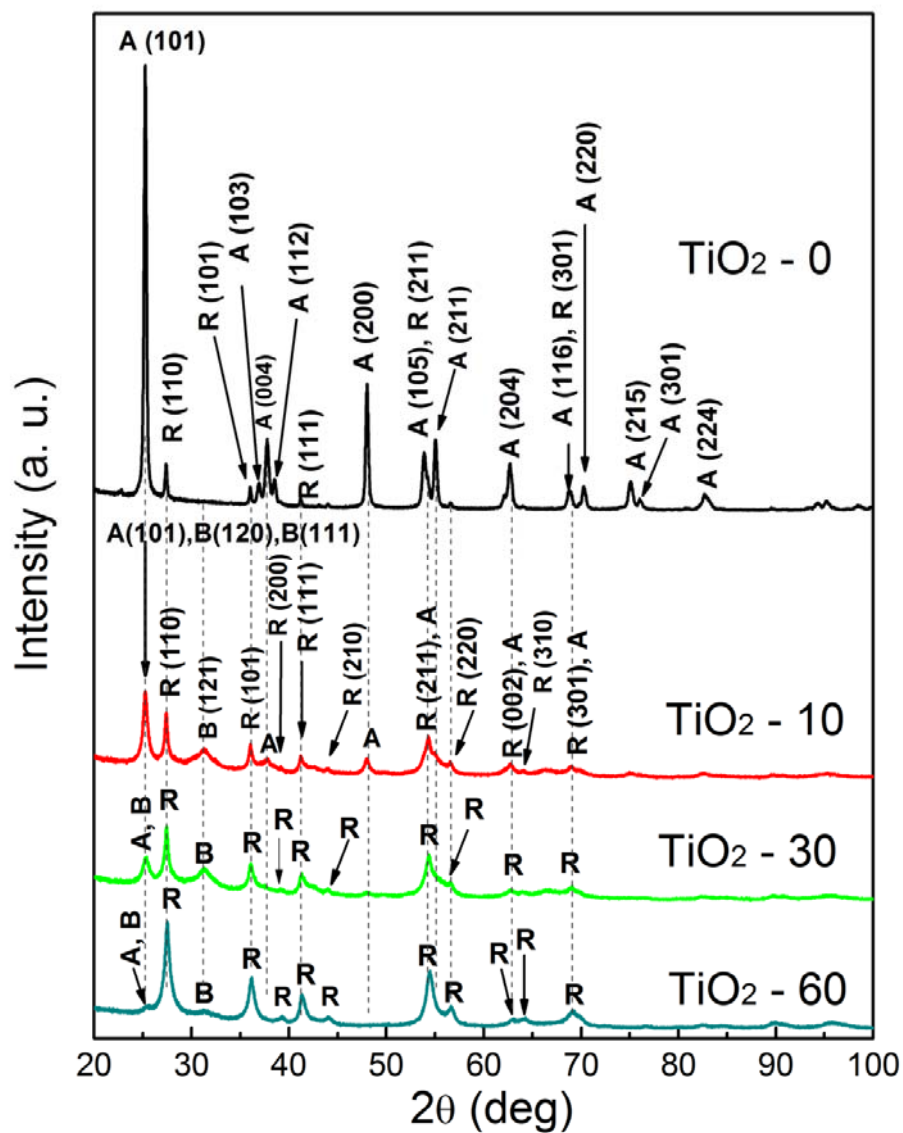| Sample | $S_{BET}$ $(m^2g^{-1})$ | $V_{tot}$ $(cm^3g^{-1})$ | $V_{meso}$ $(cm^3g^{-1})$ | $V_{micro}$ $(cm^3g^{-1})$ | $D_{mean}$ (nm) | $D_{max}$ (nm) |
|---|---|---|---|---|---|---|
| $TiO_2$-0 | 29.3 | 0.2018 | 0.1996 | 0.0075 | 20.6 | 18.0 |
| $TiO_2$-10 | 37.0 | 0.0829 | 0.0795 | 0.0123 | 9.08 | 3.90 |
| $TiO_2$-30 | 34.8 | 0.0684 | 0.0639 | 0.0119 | 8.53 | 3.80 |
| $TiO_2$-60 | 34.2 | 0.0778 | 0.0738 | 0.0093 | 8.09 | 3.17 |

Figure 1. XRD patterns of non-activated and mechanically activated $TiO_2$ (A – anatase, R – rutile, B – brookite)
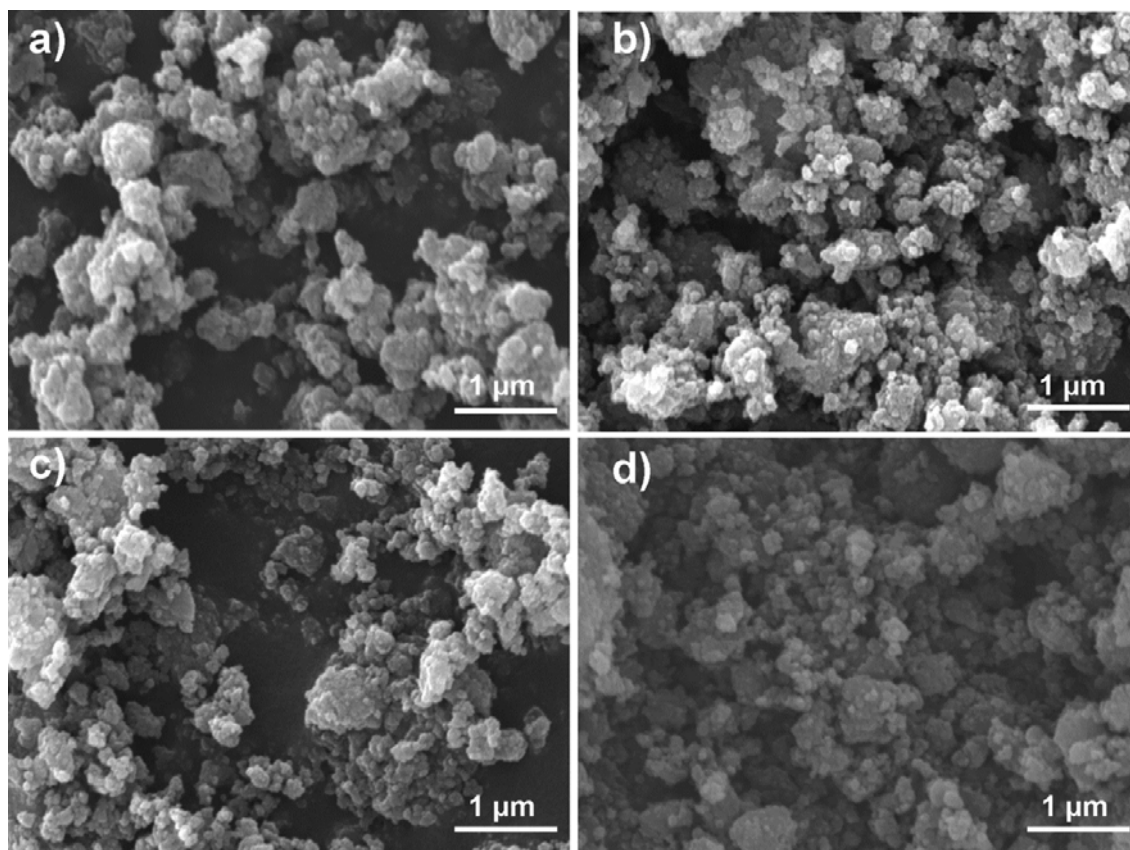
Figure 2. SEM micrographs of $TiO_2$-0 (a), $TiO_2$-10 (b), $TiO_2$-30 (c) and $TiO_2$-60 (d)
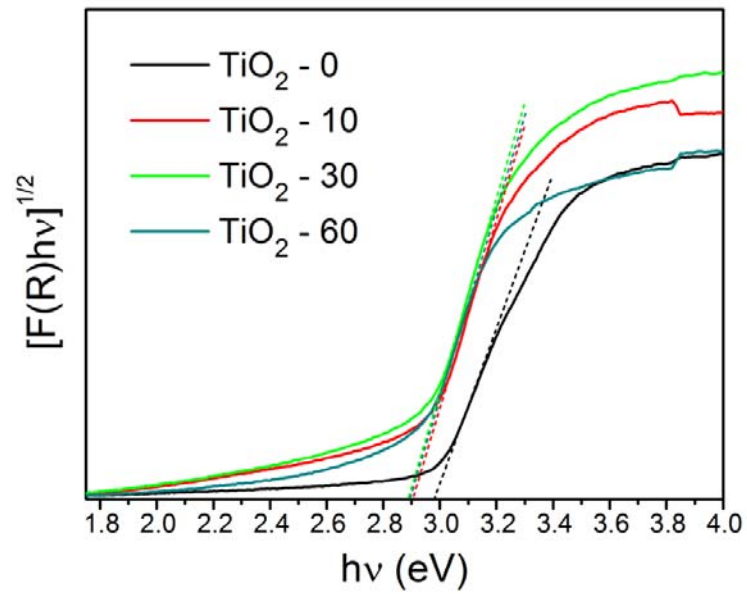
Figure 3. Tauc plot of the transformed Kubelka-Munk function versus photon energy, for non-activated and mechanically activated $TiO_2$
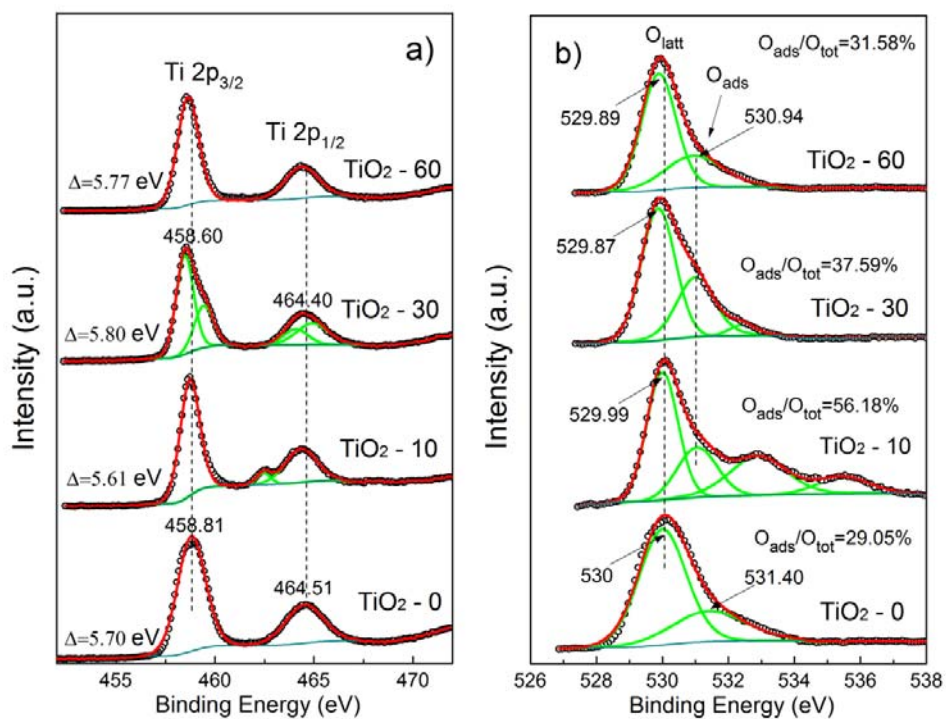
Figure 4. a) Ti 2p and b) O 1s high resolution XPS spectra of non-activated and mechanically activated $TiO_2$. Mark $\Delta$ stands for $BE(2p_{1/2})$-$BE(2p_{3/2})$, while marks $O_{latt}$, $O_{ads}$ and $O_{tot}$ refer to the lattice oxygen, surface oxygen species and total oxygen in the material, respectively
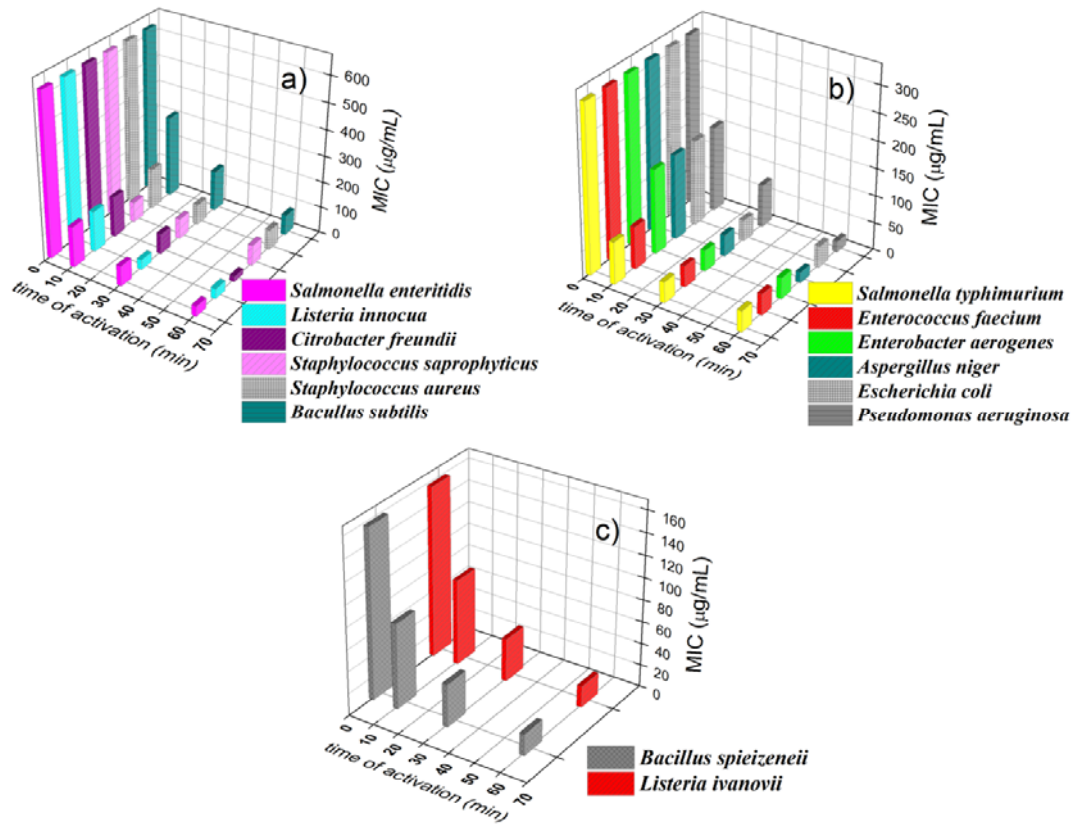
Figure 5. The influence of the mechanical activation of TiO$_2$ on the MIC values of the extract and cirsimarin against the tested microorganisms